



PERGAMON

International Journal of Non-Linear Mechanics 38 (2003) 739–751

INTERNATIONAL JOURNAL OF

**NON-LINEAR
MECHANICS**

www.elsevier.com/locate/ijnonlinmec

Attractors of a rotating viscoelastic beam

M. Abolghasemi^a, M.A. Jalali^{b,*}

^a*Aerospace Research Institute, P.O. Box 15875-3885, Tehran, Iran*

^b*Institute for Advanced Studies in Basic Sciences, P.O. Box 45195-159, Zanjan, Iran*

Abstract

We investigate the non-linear oscillations of a rotating viscoelastic beam with variable pitch angle. The governing equations of motion are two coupled partial differential equations for the longitudinal and transversal displacements. Using a perturbation technique and Galerkin's projection, we reduce the equations of motion to a non-autonomous ordinary differential equation. Our regular perturbation technique is based on the expansion of longitudinal displacement and the amplitude of first transversal mode in terms of a small parameter. We numerically generate the Poincaré maps of the reduced equations and reveal that the system exhibits regular and chaotic attractors. The regular attractors are stable limit-cycles that are relevant to stable, short-period oscillations of the beam. A bifurcation analysis has also been performed when the pitch angle is constant. © 2002 Elsevier Science Ltd. All rights reserved.

Keywords: Chaos; Limit cycles; Non-linear oscillations; Perturbation methods

1. Introduction

The absorption of undesirable vibrations of mechanical systems using passive and active control methods has been one of the important disciplines in recent years. Any control strategy needs a complete analysis of the dynamical response of the system under investigation. Amongst man-made vehicles, helicopters are subjected to very complicated aerodynamical and inertial forces, which cause the discomfort of passengers and substantial environmental noise. Having an accurate model for the dynamics of blades [1], one would be able to design a proper controller to prevent the transfer of vibrational forces to fuselage and passenger cabin [2]. Helicopter blades belong to a general class of flexible multibody systems with hybrid equations

of motion [3,4]. Linear analysis does not usually provide us a fair understanding of such systems although we enjoy the benefit of mathematical simplicity.

Jalali and Mehri [5] investigated the dynamics of a flexible crank-rocker mechanism whose governing equations were reduced to a Duffing oscillator with time-varying coefficients. Their study revealed the importance of resonances in the long-time behavior of dynamical equations. Following a similar procedure, Esmailzadeh and Jalali [6] studied the non-linear response of rectangular viscoelastic plates to base excitation and reported that stable periodic orbits can be used to determine the equivalent structural damping coefficient. In this paper, we extend the procedure of [5] to the non-linear oscillations of a rotating viscoelastic beam that can be considered as a simple model of helicopter blades in the absence of aerodynamical forces. Our goal is to investigate how a rotating beam responds to the variability of the pitch

* Corresponding author.

E-mail address: jalali@iasbs.ac.ir (M.A. Jalali).

angle. We consider non-linear strain–displacement relations and take further steps towards the understanding of spatio-temporal chaos and attractors. In Section 2, we find the governing equations of motion using Hamilton’s principle. In Section 3, we introduce proper eigenfunctions that specify the approximate shape of the deformed beam versus the spatial coordinate x , which is measured in the longitudinal direction. Using a new perturbative approach in Section 4, we determine the asymptotic solutions of the governing equations by reducing partial differential equations to ordinary ones using Galerkin’s projection. We express the zeroth- and first-order solutions in terms of a small parameter (dimensionless damping coefficient) for elastic and viscoelastic media, respectively. We also show that stable limit-cycles do exist for the system under investigation both in the absence and in the presence of structural damping. We confirm our results with the predictions of Liouville’s theorem.

2. Equations of motion

Consider a rotating beam as shown in Fig. 1. Ω is the angular velocity of the main shaft and r is the radius of the hub. The deflection of the beam is negligible in the y -direction because of the high area moment about the z -axis. Hence, we investigate the longitudinal and transversal displacements in the directions of x and z , respectively. We define the pitch angle $p(t)$ as the rotation of the beam about the x -axis. The variable $p(t)$ is adjusted with the aim of preventing helicopter blades from stalling during the retrieving motion [7].

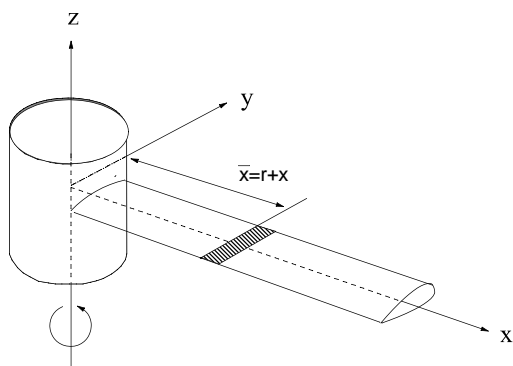


Fig. 1. A rotating beam attached to a hub of radius r .

Assume an element of the beam at the distance $\bar{x} = r + x$ from the axis of rotation. The components of the velocity vector for the chosen element are expressed by

$$\begin{aligned} v_x &= \dot{u} + w\Omega \sin p, \\ v_y &= (r + x + u)\Omega \cos p - w\dot{p}, \\ v_z &= \dot{w} - (r + x + u)\Omega \sin p, \end{aligned} \tag{1}$$

where $\dot{s} \equiv \partial s / \partial t$. The variables u and w are the longitudinal and transversal displacements, respectively. The admissible variations of v_x, v_y and v_z can be derived from (1) as

$$\begin{aligned} \delta v_x &= \delta \dot{u} + \Omega \sin p \delta w, \\ \delta v_y &= -\dot{p} \delta w + \Omega \cos p \delta u, \\ \delta v_z &= \delta \dot{w} - \Omega \sin p \delta u, \end{aligned} \tag{2}$$

where δ is the variation symbol. The functions $p(t)$ and $\dot{p}(t)$ do not admit any variation, for they are specified periodic functions of time. Thus, the variation of kinetic energy becomes

$$\delta T = \int_0^l \rho (v_x \delta v_x + v_y \delta v_y + v_z \delta v_z) dx, \tag{3}$$

with l and ρ being the length and density per unit length of the beam, respectively. By substituting from (1) and (2) into (3) one obtains

$$\begin{aligned} \delta T &= \int_0^l \rho \{ [\delta \dot{u} + \Omega \sin p \delta w][\dot{u} + w\Omega \sin p] \\ &\quad + [-\dot{p} \delta w + \Omega \cos p \delta u] \\ &\quad \times [(r + x + u)\Omega \cos p - w\dot{p}] \\ &\quad + [\delta \dot{w} - \Omega \sin p \delta u] \\ &\quad \times [\dot{w} - (r + x + u)\Omega \sin p] \} dx. \end{aligned} \tag{4}$$

We assume the following strain–displacement relation [5,8]

$$\varepsilon_x = \frac{\partial u}{\partial x} - z \frac{\partial^2 w}{\partial x^2} + \frac{1}{2} \left(\frac{\partial w}{\partial x} \right)^2, \tag{5}$$

and determine the variation of strain energy as

$$\delta U = \int_D \sigma_x \delta \varepsilon_x dD, \tag{6}$$

where D stands for the domain of extension of the beam. Let $\sigma_x = E\varepsilon_x + \eta\dot{\varepsilon}_x$, which is Kelvin’s model of viscoelastic materials [9]. The parameter E denotes the modulus of elasticity and η is the structural damping coefficient. It is noted that δU is the virtual work of both conservative and non-conservative internal forces. By applying Eqs. (4) and (6) in Hamilton’s extended principle

$$\int_{t_1}^{t_2} (\delta T - \delta U) dt = 0 \tag{7}$$

the governing equations of motion are obtained as

$$\begin{aligned} \rho[-u_{,tt} - 2\Omega(w \sin p)_{,t} + \Omega^2(r + x + u)] \\ + A\{E[u_{,xx} + w_{,x}w_{,xx}] + \eta[u_{,xxt} + \frac{1}{2}(w_{,x}^2)_{,xt}]\} = 0 \end{aligned} \tag{8}$$

and

$$\begin{aligned} \rho[2\Omega \sin pu_{,t} + (\Omega^2 \sin^2 p + p_{,t}^2)w - w_{,tt}] \\ + E[Au_{,xx}w_{,x} + Au_{,x}w_{,xx} - Iw_{,xxxx} + \frac{3}{2}Aw_{,x}^2w_{,xx}] \\ + \eta[A(w_{,x}^3)_{,xt} - Iw_{,xxxxt} + A(u_{,xt}w_{,x})_{,x}] = 0, \end{aligned} \tag{9}$$

where I and A are the area moment and cross-sectional area of the beam, respectively. It is assumed that the first area moment is zero, which is valid for symmetric cross-sections. The abbreviation $_{,v}$ denotes a partial derivative with respect to v . For a beam clamped to the hub, the following boundary conditions hold at $x = 0$ and $x = l$:

$$u = 0 \quad \text{at} \quad x = 0, \tag{10}$$

$$w = w_{,x} = 0 \quad \text{at} \quad x = 0, \tag{11}$$

$$I \left(E + \eta \frac{\partial}{\partial t} \right) w_{,xx} = 0 \quad \text{at} \quad x = l, \tag{12}$$

$$u_{,x} + \frac{1}{2}w_{,x}^2 = 0 \quad \text{at} \quad x = l, \tag{13}$$

$$I \left(E + \eta \frac{\partial}{\partial t} \right) w_{,xxx} = 0 \quad \text{at} \quad x = l, \tag{14}$$

which are the other consequences of (7).

3. Shape functions

Eqs. (8) and (9) along with the boundary conditions (10)–(14) describe a set of non-linear, non-autonomous partial differential equations for which closed-form solutions are not known. We attempt to solve these equations through expanding w by the series

$$w(x, t) = \sum_{n=1}^N w_n(x, t). \tag{15}$$

We assume $w_n(x, t) = \phi_n(t)\psi_n(x)$ and determine the *shape functions* $\psi_n(x)$ using the linear part of (9)

$$w_{,tt} + \lambda^2 w_{,xxxx} = 0, \quad \lambda^2 = \frac{EI}{\rho}. \tag{16}$$

This equation, can readily be solved by the method of separation of variables. One finds out

$$\begin{aligned} \psi_n(x) = [\sinh(\beta_n x) - \sin(\beta_n x)] \\ - \frac{\sinh(\beta_n l) + \sin(\beta_n l)}{\cosh(\beta_n l) + \cos(\beta_n l)} \\ \times [\cosh(\beta_n x) - \cos(\beta_n x)] \end{aligned} \tag{17}$$

in which the *eigenvalues* β_n are computed through solving

$$1 + \cos(\beta_n l) \cosh(\beta_n l) = 0. \tag{18}$$

We call $\phi_n(t)$ as *amplitude* functions. In this study, we confine ourselves to the fundamental (first) mode, $n = 1$, for most part of the kinetic energy is carried by this mode [10], and introduce a perturbation technique to determine the longitudinal displacement $u(x, t)$ as well as the amplitude function of the fundamental mode, $\phi(t) \equiv \phi_1(t)$. To find an appropriate perturbation parameter, we consider free longitudinal vibration of the beam represented by

$$EAu_{,xx} + \eta Au_{,xxt} - \rho u_{,tt} = 0, \tag{19}$$

with the associated boundary conditions $u(0, t) = 0$ and $\sigma_x(l, t) = 0$. We assume $u(x, t) = X(x)\mathcal{F}(t)$, which after substituting in (19) and employing the boundary conditions, yields

$$\frac{d^2 \mathcal{F}}{dt^2} + \frac{\eta \omega_n^2}{E} \frac{d \mathcal{F}}{dt} + \omega_n^2 \mathcal{F} = 0, \tag{20}$$

where

$$\omega_n^2 = \frac{EA\lambda_n^2}{\rho}, \quad \lambda_n = \frac{(2n-1)\pi}{2l}, \tag{21}$$

and n is the mode number. We now set $n=1$ and define $\eta = 2\zeta E/\omega_n$, where ζ is the dimensionless damping coefficient. The characteristic equation of (20) will have the roots $s_{1,2} = -\zeta\omega_1 \pm \omega_1(\zeta^2 - 1)^{1/2}$. For an underdamped oscillatory system, we need $\zeta^2 < 1$. Hence, ζ can serve as a perturbation parameter.

4. Perturbed equations

For slender beams, the inertia forces along the longitudinal direction become negligible in comparison with those of the lateral ones. Therefore, one can suppose that $u_{tt} \approx 0$ (see also [8]). By this assumption, Eq. (8) reads

$$\begin{aligned} &\rho[-2\Omega(w \sin p)_{,t} + \Omega^2(r+x+u)] \\ &+ EA \left\{ [u_{,xx} + w_{,x}w_{,xx}] \right. \\ &\left. + \frac{2\zeta}{\omega_1} \left[u_{,xxt} + \frac{1}{2}(w_{,x}^2)_{,xt} \right] \right\} = 0, \tag{22} \end{aligned}$$

which should be solved along with (9). We use a regular perturbation method and expand $u(x, t)$ and $\phi(t)$ in terms of the small parameter ζ . i.e.,

$$u(x, t) = \sum_{j=0}^{\infty} \zeta^j u_j(x, t), \tag{23}$$

$$w_1(x, t) = \psi(x)\phi(t), \tag{24}$$

$$\phi(t) \equiv \phi_1(t) = \sum_{j=0}^{\infty} \zeta^j F_j(t), \quad \psi(x) \equiv \psi_1(x), \tag{25}$$

for $\zeta \ll 1$. We first substitute from (23) and (24) into Eqs. (9) and (22). This gives us

$$\begin{aligned} &\rho \left\{ \left[-2\Omega\psi \sin p \sum_{j=0}^{\infty} \zeta^j F_j \right]_{,t} \right. \\ &\left. + \Omega^2 \left[r+x + \sum_{j=0}^{\infty} \zeta^j u_j(x, t) \right] \right\} \end{aligned}$$

$$\begin{aligned} &+ EA \left[\sum_{j=0}^{\infty} \zeta^j u_{j,xx}(x, t) + \beta^3 \psi_{,y} \psi_{,yy} \left(\sum_{j=0}^{\infty} \zeta^j F_j \right)^2 \right] \\ &+ \frac{2EA\zeta}{\omega_1} \left[\sum_{j=0}^{\infty} \zeta^j u_{j,xxt}(x, t) \right. \\ &\left. + 2\beta^3 \psi_{,y} \psi_{,yy} \sum_{i=0}^{\infty} \zeta^i \dot{F}_i \sum_{j=0}^{\infty} \zeta^j F_j \right] = 0 \tag{26} \end{aligned}$$

and

$$\begin{aligned} &\rho \left\{ 2\Omega \sin p \sum_{j=0}^{\infty} \zeta^j u_{j,t} + \psi[\Omega^2 \sin^2 p + \dot{p}^2] \right. \\ &\left. \times \sum_{j=0}^{\infty} \zeta^j F_j - \psi \sum_{j=0}^{\infty} \zeta^j \ddot{F}_j \right\} \\ &+ E \left\{ A \left[\beta \psi_{,y} \sum_{j=0}^{\infty} \zeta^j u_{j,xx} + \beta^2 \psi_{,yy} \sum_{j=0}^{\infty} \zeta^j u_{j,x} \right. \right. \\ &\left. \left. + \frac{3}{2} \beta^4 \psi_{,y}^2 \psi_{,yy} \left(\sum_{j=0}^{\infty} \zeta^j F_j \right)^2 \right] - I\beta^4 \psi_{,yyy} \right\} \sum_{j=0}^{\infty} \zeta^j F_j \\ &+ \frac{2E\zeta}{\omega_1} \left\{ 9A\beta^4 \psi_{,yy} \psi_{,y}^2 \sum_{i=0}^{\infty} \zeta^i \dot{F}_i \left(\sum_{j=0}^{\infty} \zeta^j F_j \right)^2 \right. \\ &\left. - I\beta^4 \psi_{,yyyy} \sum_{j=0}^{\infty} \zeta^j \dot{F}_j(t) \right. \\ &\left. + A \left[\beta \psi_{,y} \sum_{j=0}^{\infty} \zeta^j u_{j,xxt} + \beta^2 \psi_{,yy} \sum_{j=0}^{\infty} \zeta^j u_{j,xt} \right] \right. \\ &\left. \times \sum_{j=0}^{\infty} \zeta^j F_j \right\} = 0, \tag{27} \end{aligned}$$

where $y = \beta x$ and $\beta \equiv \beta_1 = 1.875/l$. We then collect the coefficients of similar powers of ζ in order to recursively determine $u_0(x, t)$, $F_0(t)$, $u_1(x, t)$, $F_1(t)$, etc. In this paper, we generate first-order solutions of

the form

$$u(x, t) \approx u_0(x, t) + \zeta u_1(x, t),$$

$$w_1(x, t) \approx \psi(x)[F_0(t) + \zeta F_1(t)], \quad (28)$$

which are adequate to explore short-period motions and the long-term behavior of the system as $\zeta \rightarrow 0$.

5. Zeroth-order solutions

The coefficients of ζ^0 in (26) and (27) are

$$u_{0,xx} + \frac{\rho\Omega^2}{EA}u_0 - \frac{\rho}{EA}[2\Omega w_{10,t} \sin p + 2\Omega w_{10} \dot{p} \cos p - \Omega^2(r+x)] + w_{10,x}w_{10,xx} = 0, \quad (29)$$

and

$$\rho\{2\Omega u_{0,t} \sin p + [\Omega^2 \sin^2 p + \dot{p}^2]w_{10}(x, t) - w_{10,tt}\} + E[Au_{0,xx}w_{10,x} + Au_{0,x}w_{10,xx} + \frac{3}{2}A(w_{10,x})^2w_{10,xx} - Iw_{10,xxxx}] = 0, \quad (30)$$

with $w_{10}(x, t) = \psi(x)F_0(t)$. We can rewrite (29) as

$$u_{0,xx} + Cu_0 = f_0(x, t), \quad (31)$$

where

$$f_0(x, t) = D[2\Omega w_{10,t} \sin p + 2\Omega w_{10} \dot{p} \cos p - \Omega^2(r+x)] - w_{10,x}w_{10,xx}, \quad (32)$$

$$C = \frac{\rho\Omega^2}{EA}, \quad D = \frac{\rho}{EA}. \quad (33)$$

Eq. (31) is an inhomogeneous ordinary differential equation (ODE) for u_0 in terms of x . The general homogeneous solution of (31) is expressed by

$$u_0^h(x, t) = A_0(t) \cos(\sqrt{C}x) + B_0(t) \sin(\sqrt{C}x) \quad (34)$$

from which a particular solution can be found by applying Lagrange's method of the variation of parameters as

$$u_0^p(x, t) = -\frac{\cos(\sqrt{C}x)}{\sqrt{C}} \int_0^x \sin(\sqrt{C}s) f_0(s, t) ds + \frac{\sin(\sqrt{C}x)}{\sqrt{C}} \int_0^x \cos(\sqrt{C}s) f_0(s, t) ds. \quad (35)$$

The general solution $u_0(x, t)$ is the sum of u_0^h and u_0^p in which $A_0(t)$ and $B_0(t)$ are obtained by employing the boundary conditions (10) and (13). We get $A_0(t) = 0$ and

$$B_0(t) = -\frac{\tan(\sqrt{C}l)}{\sqrt{C}} \{[\dot{F}_0 \sin p + F_0 \dot{p} \cos p] \mathcal{S}_1(l) + \mathcal{S}_2(l) - F_0^2 \mathcal{S}_3(l)\} - \frac{1}{\sqrt{C}} \{[\dot{F}_0 \sin p + F_0 \dot{p} \cos p] \mathcal{C}_1(l) + \mathcal{C}_2(l) - F_0^2 \mathcal{C}_3(l)\} - \frac{F_0^2 \beta^2 \psi_y^2(l)}{2\sqrt{C} \cos(\sqrt{C}l)}. \quad (36)$$

The functions \mathcal{S}_j and \mathcal{C}_j ($j=1, 2, 3$) are introduced in Appendix A. In practical applications, the pitch angle $p(t)$ is a periodic function as [7]

$$p(t) = p_0[1 + \cos(\Omega t)], \quad (37)$$

with p_0 being a constant. By calculating the partial derivatives of u_0 with respect to x and t and substituting the results into (30) we obtain the following partial differential equation (PDE):

$$\Theta_1(x, t) \ddot{F}_0 + \Theta_2(x, t) F_0 \dot{F}_0 + \Theta_3(x, t) \dot{F}_0 + \Theta_4(x, t) F_0^3 + \Theta_5(x, t) F_0^2 + \Theta_6(x, t) F_0 = 0, \quad (38)$$

where

$$\Theta_1(x, t) = \rho[2\Omega R_1(x) \sin^2 p - \psi(x)], \quad (39)$$

$$\Theta_2(x, t) = -2\rho\Omega \sin p [2R_2(x) + R_3(x)] + EA \sin p [R_4(x) + R_7(x)], \quad (40)$$

$$\Theta_3(x, t) = 4\rho\Omega \dot{p} \sin p \cos p R_1(x), \quad (41)$$

$$\Theta_4(x, t) = -EA[R_5(x) + R_8(x) + \frac{3}{2}\beta^4 \psi_{,yy}], \quad (42)$$

$$\Theta_5(x, t) = EA \dot{p} \cos p [R_4(x) + R_7(x)], \quad (43)$$

$$\Theta_6(x, t) = \rho \left[\Omega \sin p \frac{\partial}{\partial t} (\dot{p} \cos p) R_1(x) + (\Omega^2 \sin^2 p + \dot{p}^2) \psi(x) \right] + EA[R_6(x) + R_9(x)] - EI\beta^4 \psi_{,yyyy}. \quad (44)$$

The functions $R_j(x)$ ($j = 1, \dots, 9$) have been given in Appendix B. Eq. (38) can be reduced to an ODE by removing the space coordinate x using Galerkin's global averaging method [11]. To achieve this goal, we multiply (38) by $\psi(x)$ and integrate the resulting equation over x from 0 to l . This yields

$$\dot{y}_1 = g_1(y_1, y_2, t) = y_2,$$

$$\begin{aligned} \dot{y}_2 = g_2(y_1, y_2, t) = & -q_1(t)y_1y_2 - q_2(t)y_2 \\ & - q_3(t)y_1^3 - q_4(t)y_1^2 - q_5(t)y_1 = 0, \end{aligned} \quad (45)$$

where $y_1 = F_0$, $y_2 = \dot{F}_0$ and

$$q_i(t) = \frac{\xi_{i+1}(t)}{\xi_1(t)}, \quad i = 1, \dots, 5, \quad (46)$$

$$\xi_i(t) = \int_0^l \Theta_i(x, t) \psi(x) dx, \quad i = 1, \dots, 6. \quad (47)$$

$q_i(t)$ are $2\pi/\Omega$ -periodic functions of time.

Applying Liouville's theorem to (45) results in [12]

$$\frac{1}{V} \frac{dV}{dt} = \nabla \cdot g = \frac{\partial g_1}{\partial y_1} + \frac{\partial g_2}{\partial y_2} = -q_2(t) - q_1(t)y_1, \quad (48)$$

where $g = (g_1, g_2)^T$ and V denotes the volume of an arbitrary phase space element. For the systems with $\nabla \cdot g = 0$, the phase space equations can be written as

$$\dot{z} = \mathcal{J} \cdot \frac{\partial \mathcal{H}}{\partial z}, \quad (49)$$

where z is the vector of state variables, \mathcal{J} is the so-called symplectic matrix [13] and \mathcal{H} is the Hamiltonian function. All fixed points of (49) are of center and saddle type. As Eq. (48) shows, $\nabla \cdot g$ can take both positive and negative values in our model. Therefore, the phase space of (45) has not necessarily a symplectic structure (the existence of the Hamiltonian \mathcal{H} is not guaranteed) and some regular or chaotic limit sets are expected to emerge. Such a phenomenon is observed in the van der Pol oscillator that has a stable limit-cycle. Below, we investigate the behavior of (45) and determine regular and chaotic attractors numerically.

5.1. Poincaré maps

The phase space of equations (45) is three dimensional (taking into account t as the third state variable).

So, to visualize the phase space flows, we have generated the Poincaré map of this system by sampling $y_1(t)$ and $y_2(t)$ with the time step $2\pi/\Omega$ (this is the period of $q_i(t)$). The constant parameters have been set to $a=0.01$ (m), $b=0.007$ (m), $I=ab^3/12$, $A=ab$, $E=207 \times 10^9$ (Pa), $\rho=7500$ (kg/m³), $r=0.08$ (m), $p_0=\pi/12$ and $l=0.4$ (m). Fig. 2a and b show the surfaces of section for $\Omega=50$ and $\Omega=100$ (rpm), respectively. Two main fixed points can be distinguished in these figures. The point A is a stable focus that attracts the trajectories between the boundary curves Γ_1 and Γ_2 (see Fig. 2b). The point B is an elliptic fixed point around which quasi-periodic orbits occur. Quasi-periodic orbits are bound to the boundary curve Γ_1 . The trajectories outside Γ_2 belong to the set of high resonant and chaotic orbits, and diffuse in the phase space quickly. On the evidence of Fig. 2a and b, by increasing the value of Ω , the number of quasi-periodic islands decreases and stochastic orbits dominate the outer regions. The point A is a stable limit-cycle of period $T=2\pi/\Omega$. The quantity $\nabla \cdot g$ eventually becomes negative (Fig. 2c) for the trajectories between Γ_1 and Γ_2 , which are attracted to A. For the trajectories enclosed by Γ_1 , the orbital average of $\nabla \cdot g$ (over the period T) is zero indicating that the stable tori around B belong to a family of symplectic manifolds (see Fig. 2d). $\nabla \cdot g$ has not a definite sign for stochastic orbits. The results reported above are altered if we continue the solution procedure up to the first-order terms in ζ . This is the subject of the next section.

6. First-order solutions

First-order solutions are found by determining $u_1(x, t)$ and $w_{11}(x, t) = \psi(x)F_1(t)$ in (28). We collect the coefficients of ζ^1 in Eqs. (26) and (27) that become

$$u_{1,xx} + Cu_1 = f_1(x, t) \quad (50)$$

and

$$\begin{aligned} \rho \{ 2\Omega \sin pu_{1,t} + [\Omega^2 \sin^2 p + \dot{p}^2] F_1 \psi(x) \\ - \ddot{F}_1 \psi(x) \} + E \{ Au_{0,xx} [F_1 \beta \psi_{,y}] + Au_{1,xx} [F_0 \beta \psi_{,y}] \\ + Au_{0,x} [F_1 \beta^2 \psi_{,yy}] + Au_{1,x} [F_0 \beta^2 \psi_{,yy}] \} \end{aligned}$$

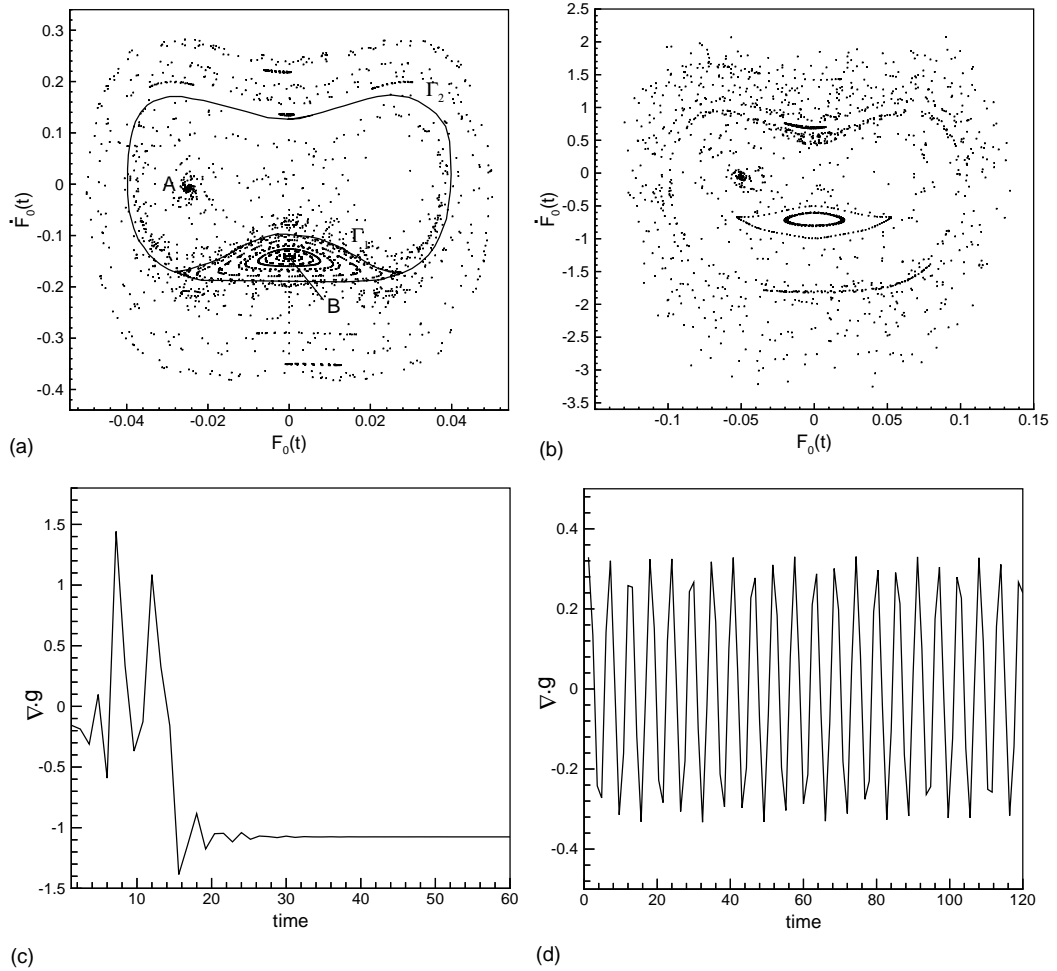


Fig. 2. The numerically generated Poincaré maps of the zeroth-order solutions with the sampling time $T = 2\pi/\Omega$. Panels (a) and (b) correspond to $\Omega = 50$ and $\Omega = 100$ (rpm), respectively, (c) The time history of $\nabla \cdot g$ for a trajectory that is attracted to A, (d) The time history of $\nabla \cdot g$ for a quasi-periodic orbit enclosed by Γ_1 . The average of $\nabla \cdot g$ is zero over one period $T = 2\pi/\Omega$.

$$\begin{aligned}
 & -IF_1\beta^4\psi_{,yyyy} + \frac{3}{2}A[F_0\beta\psi_{,y}]^2[F_1\beta^2\psi_{,yy}] \\
 & + 3A[F_0\beta\psi_{,y}][F_0\beta^2\psi_{,yy}][F_1\beta\psi_{,y}] \\
 & + \frac{2E}{\omega_1}\{3A[\dot{F}_0\beta^2\psi_{,yy}][F_0\beta\psi_{,y}]^2 \\
 & + 6A[F_0\beta^2\psi_{,yy}][\dot{F}_0\beta\psi_{,y}][F_0\beta\psi_{,y}] - I\dot{F}_0\beta^4\psi_{,yyyy} \\
 & + Au_{0,xx}[F_0\beta\psi_{,y}] + Au_{0,xt}[F_0\beta^2\psi_{,yy}]\} = 0, \quad (51)
 \end{aligned}$$

where

$$\begin{aligned}
 f_1(x, t) = 2D\Omega[\sin p\dot{F}_1 + F_1\dot{p} \cos p]\psi(x) \\
 - 2[F_0F_1\beta^3\psi_{,y}\psi_{,yy}] - K[u_{0,xt} \\
 + 2\dot{F}_0F_0\beta^3\psi_{,y}\psi_{,yy}], \quad (52)
 \end{aligned}$$

$$K = \frac{2}{\omega_1}. \quad (53)$$

The functions $w_{10}(x, t) = F_0(t)\psi(x)$ and $u_0(x, t)$ have been found as the zeroth-order solutions and are supplied to Eqs. (50) and (51). Eq. (50) is an

inhomogeneous linear ODE for $u_1(x, t)$ in terms of x the solution of which is expressed by

$$u_1(x, t) = A_1(t) \cos(\sqrt{C}x) + B_1(t) \sin(\sqrt{C}x) - \frac{\cos(\sqrt{C}x)}{\sqrt{C}} \int_0^x \sin(\sqrt{C}s) f_1(s, t) ds + \frac{\sin(\sqrt{C}x)}{\sqrt{C}} \int_0^x \cos(\sqrt{C}s) f_1(s, t) ds, \quad (54)$$

where $A_1(t)$ and $B_1(t)$ are determined using the boundary conditions on u as

$$A_1(t) = 0, \quad (55)$$

$$B_1(t) = -\frac{\tan(\sqrt{C}l)}{\sqrt{C}} \int_0^l \sin(\sqrt{C}s) f_1(s, t) ds - \frac{1}{\sqrt{C}} \int_0^l \cos(\sqrt{C}s) f_1(s, t) ds - \frac{F_0 F_1 \beta^2 \psi_{,y}^2(l)}{\sqrt{C} \cos(\sqrt{C}l)}. \quad (56)$$

After calculating the partial derivatives of $u_1(x, t)$ and carrying out some algebraic manipulation, Eq. (51) is transformed to

$$\Theta_1(x, t) \ddot{F}_1 + \Theta_2(x, t) \dot{F}_1 + \Theta_3(x, t) F_1 + \Theta_4(x, t) = 0 \quad (57)$$

with

$$\Theta_1(x, t) = \rho[2\Omega \sin^2 p K_9(x) - \psi(x)], \quad (58)$$

$$\Theta_2(x, t) = 4\Omega\rho \sin p [\dot{p} \cos p K_9(x) - 2F_0 K_{10}(x)] + EAF_0 \sin p [\beta \psi_{,y} K_5(x) + \beta^2 \psi_{,yy} K_1(x)], \quad (59)$$

$$\Theta_3(x, t) = 2\rho\Omega \sin p \left[\frac{\partial}{\partial t} (\dot{p} \cos p) K_9(x) - 2\dot{F}_0 K_{10}(x) \right] + \rho(\Omega^2 \sin^2 p + \dot{p}^2) \psi(x) + EA\beta \psi_{,y} [u_{0,xx} - 2\dot{F}_0^2 K_6(x)] + EA\beta^2 \psi_{,yy} [u_{0,x} - 2\dot{F}_0^2 K_2(x)] - EI\beta^4 \psi_{,yyyy} + EAF_0 \dot{p} \cos p [\beta \psi_{,y} K_5(x) - \beta^2 \psi_{,yy} K_1(x)] + \frac{9}{2} EAF_0^2 \beta^4 \psi_{,y}^2 \psi_{,yy}, \quad (60)$$

$$\Theta_4(x, t) = 2\rho\Omega \sin p [-2(\ddot{F}_0 F_0 + \dot{F}_0^2) K_{11}(x) - K_{12}(x, t)] + EAF_0 \beta \psi_{,y} [-\dot{F}_0 F_0 K_7(x) - K_8(x, t)] + EAF_0 \beta^2 \psi_{,yy} [-\dot{F}_0 F_0 K_3(x) - K_4(x, t)] - \frac{2EI}{\omega_1} \dot{F}_0 \beta^4 \psi_{,yyyy} + \frac{2EA}{\omega_1} \{9\dot{F}_0 F_0^2 \beta^4 \psi_{,y}^2 \psi_{,yy} + F_0 [u_{0,xx} \beta \psi_{,y} + u_{0,xt} \beta^2 \psi_{,yy}]\}. \quad (61)$$

The functions K_j ($j = 1, \dots, 12$) are expressed in Appendix C. In the computation of these functions, we calculate $u_0(x, t)$ numerically, and then, evaluate the integrals over the x -domain. Eq. (57) can be reduced to an ODE for F_1 with time varying coefficients by applying Galerkin’s method. This leads to

$$\Delta_1(t) \ddot{F}_1 + \Delta_2(t) \dot{F}_1 + \Delta_3(t) F_1 + \Delta_4(t) = 0, \quad (62)$$

where

$$\Delta_i(t) = \int_0^l \Theta_i(x, t) \psi(x) dx. \quad (63)$$

The behavior of these functions depends on $p(t)$, $F_0(t)$ and their temporal derivatives. Our numerical experiments show that the solution of (62) becomes unstable for chaotic zeroth-order solutions. So, we confine ourselves to those regions of the phase space that result in periodic and quasi-periodic orbits of $F_0(t)$. The Poincaré map of the first-order solutions has been generated for $\Omega = 50$ (rpm) and $\zeta = 10^{-6}$ in the “sampled” $\phi-\dot{\phi}$ plane (Fig. 3a). Since $\Delta_i(t)$ are generally quasi-periodic functions of time, we set the sampling time to $2\pi/\Omega$, which is the shortest period of $F_0(t)$. This allows us to explore possible harmonic and subharmonic oscillations. As Fig. 3a shows, two stable periodic solutions (limit-cycles) attract all of the phase space trajectories. The limit-cycle corresponding to the fixed point A (see Fig. 3a) has been computed and plotted in Fig. 3b. This is a one-dimensional manifold in the $\phi-\dot{\phi}$ phase space. It is worth noting that the geometry of Fig. 3a emerges from that of Fig. 2a.

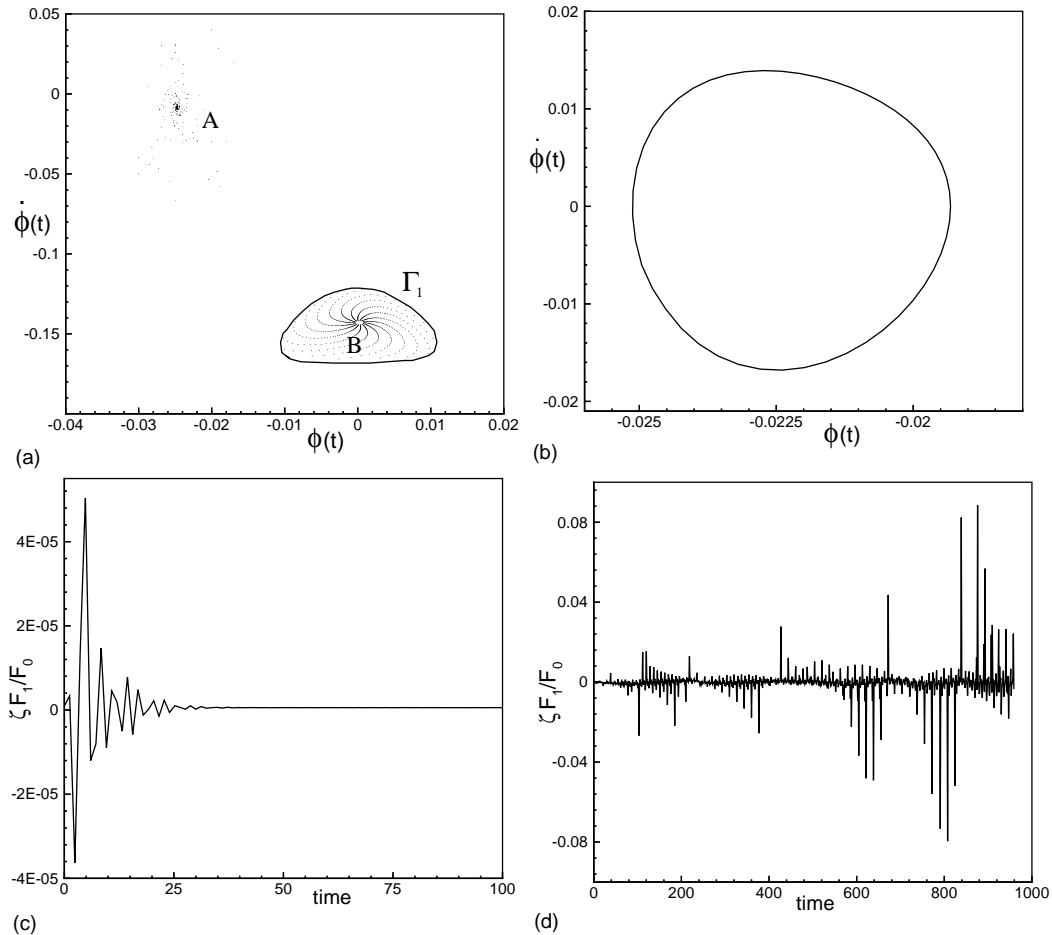


Fig. 3. (a) The numerically generated Poincaré map of the first-order solution with the sampling time $T = 2\pi/\Omega$, where $\Omega = 50$ (rpm). A similar structure appears for $\Omega = 100$, (b) The stable limit-cycle corresponding to the attracting fixed point A. Panels (c) and (d) show the variation of $\zeta F_1(t)/F_0(t)$ for sample trajectories, which are attracted to A and B, respectively. These results show that our perturbation solutions are credible.

The nature of the fixed point B is changed as dissipative terms are included in the solutions. The boundary curve Γ_1 is preserved for $\zeta \neq 0$ and separates the domains of attraction of A and B. In Fig. 3c and d, we have plotted the history of $\mathcal{P} = \zeta F_1(t)/F_0(t)$ for two sample trajectories that are attracted to the fixed points A and B. As these figures show, we have $|\mathcal{P}| \ll 1$, which is the essential requirement of our perturbation solutions. For the trajectories that are attracted to A, the zeroth-order system eventually becomes dissipative (Fig. 2c), which causes $\mathcal{P} \rightarrow 0$ as $t \rightarrow \infty$. This is not the case for the trajectories that are attracted to B (\mathcal{P} is oscillatory).

7. Discussion

As the numerical computations show, stable limit-cycles exist for both elastic and viscoelastic beams, which respectively correspond to the zeroth- and first-order solutions of the perturbed equations. This phenomenon is exceptional in structural dynamics, specially, in the oscillations of beams, plates and shells. The observed behavior is linked to the variability of the pitch angle $p(t)$ because the principal axes of the beam cross-section do not coincide with the axis of rotation for $l \neq (2n + 1)\pi/\Omega$ ($n = 0, 1, 2, \dots$). To gain a better sense about the physics of the

problem, let us assume $p = \dot{p} = 0$, which corresponds to a rotating beam with zero *angle of attack*. In such a circumstance, the functions Θ_2, Θ_3 and Θ_5 vanish in (38) leaving Eq. (45) in the form

$$\begin{aligned} \dot{y}_1 &= y_2, \\ \dot{y}_2 &= -\gamma_3 y_1^3 - \gamma_1 y_1 \end{aligned} \tag{64}$$

with γ_1 and γ_3 as constant parameters. This is the well-known Duffing's oscillator, which occurs in

the analysis of non-rotating Euler–Bernoulli beams [14,15]. It is remarked that the angular velocity Ω does not appear in the equations of motion when $p = 0$ (in such a circumstance, the angular velocity and displacement vectors lie in the same plane).

As the pitch angle varies, the coefficients of the reduced ODE become time dependent and additional terms consisting of y_2 appear in the equation of \dot{y}_2 . Thus, the phase space loses its symplectic structure. For a fixed but non-zero angle of attack ($\dot{p} = 0, p \neq 0$),

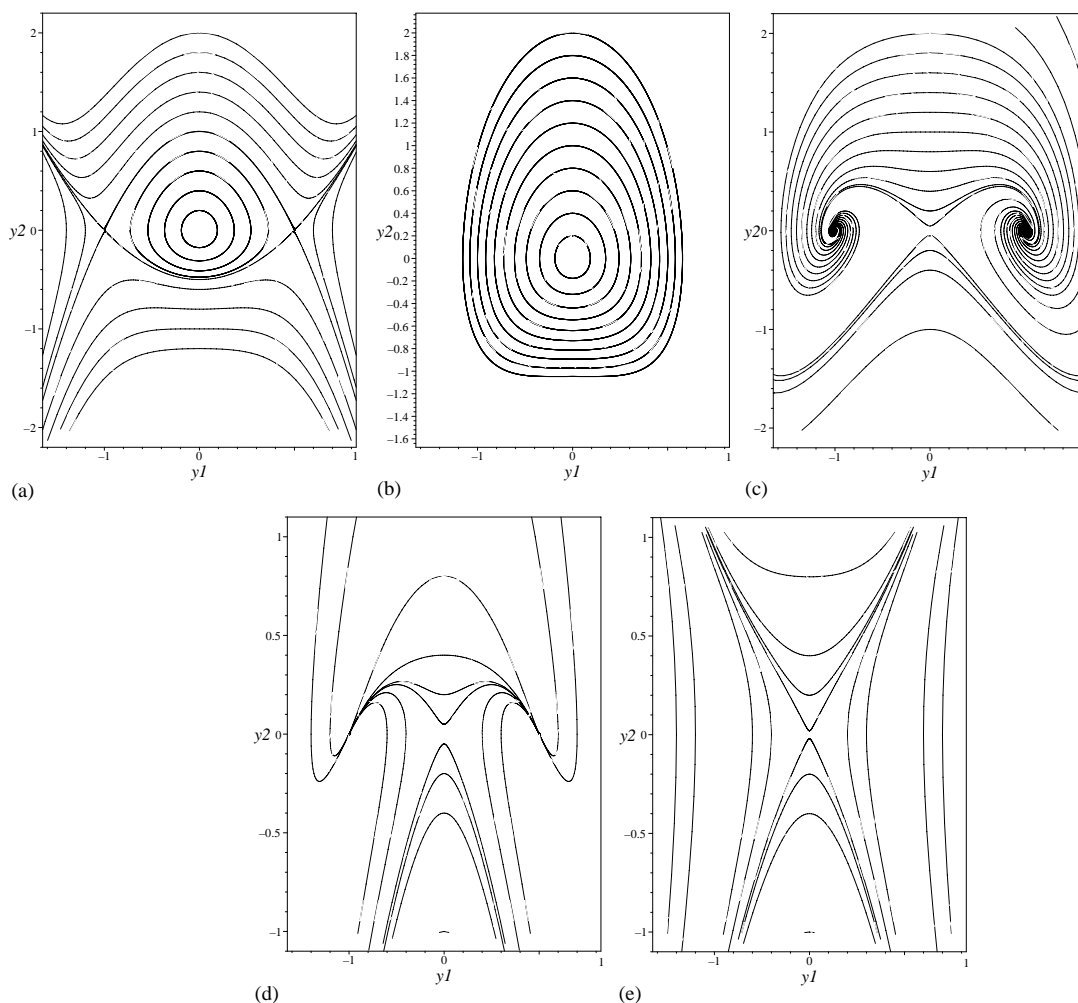


Fig. 4. Bifurcations in the phase space flows of the zeroth-order solutions for $\dot{p} = 0$ and $p \neq 0$, which correspond to a rotating beam of constant pitch angle: (a) $\gamma_1 > 0, \gamma_1 \gamma_3 < 0$ and $\Delta > 0$, (b) $\gamma_1 > 0$ and $\gamma_1 \gamma_3 > 0$, (c) $\gamma_1 < 0, \gamma_1 \gamma_3 < 0$, and $\Delta < 0$, (d) $\gamma_1 < 0, \gamma_1 \gamma_3 < 0$ and $\Delta > 0$, (e) $\gamma_1 < 0, \gamma_1 \gamma_3 > 0$.

we attain

$$\begin{aligned} \dot{y}_1 &= y_2, \\ \dot{y}_2 &= -\gamma_{12}y_1y_2 - \gamma_3y_1^3 - \gamma_1y_1, \end{aligned} \tag{65}$$

where γ_1 , γ_3 and γ_{12} are constant coefficients. Depending on the values of these parameters, the phase space flows of (65) take one of the general structures of Fig. 4. Define $\Delta = 8\gamma_1 - \gamma_{12}^2\gamma_1/\gamma_3$. As Fig. 4a shows, for $\gamma_1 > 0$, $\gamma_1\gamma_3 < 0$ and $\Delta > 0$, the origin is a center enclosed by a continuous family of periodic orbits. These orbits are bound to the heteroclinic orbits of two saddle points. Outside the region enclosed by the heteroclinic orbits, unstable solutions occur. For $\gamma_1 > 0$ and $\gamma_1\gamma_3 > 0$, all of the phase space is filled by periodic orbits (Fig. 4b). For $\gamma_1 < 0$, $\gamma_1\gamma_3 < 0$ and $\Delta < 0$, the origin is a saddle point and two spiral foci occur at $(\pm 1, 0)$. The singular point at $(-1, 0)$ is repelling, while the point $(+1, 0)$ is an attractive one. As it can be seen in Fig. 4c, the phase space is divided to two zones that are separated by the lower branches of the global invariant manifolds of the saddle point. The trajectories starting on the upper side of the boundary curve are eventually attracted to the point $(+1, 0)$. Meanwhile, the trajectories on the lower region are escaping unstable solutions. As Δ switches sign, the unstable and stable spiral foci of Fig. 4c become repelling and attracting nodes, respectively (Fig. 4d). For $\gamma_1 < 0$, $\gamma_1\gamma_3 > 0$, the origin is a saddle point and the phase space is populated by unstable solutions (Fig. 4e). It is remarked that analytical solutions are obtainable for (62) when $\dot{p} = 0$.

First-order solutions diverge when $F_0(t)$ is chaotic. This shows that structural dissipation is not always useful in the passive control of vibrating systems. Thus, an active controller is needed to damp the stochastic oscillations of rotating elastic beams (the case $\zeta = 0$). On the evidence of the generated Poincaré maps, chaotic oscillations have large amplitudes that may result in global instability of the beam through a secular change in F_0 and \dot{F}_0 . For $\dot{p} = 0$, the instability of solutions will be due to the unbounded solutions of y_1 and y_2 in (65).

Acknowledgements

We thank the anonymous referees for their useful suggestions that helped us to improve the presentation of the paper.

Appendix A. The functions \mathcal{S}_j and \mathcal{C}_j

$$\begin{aligned} \mathcal{S}_1(x) &= 2\Omega D \int_0^x \sin(\sqrt{C}s)\psi(s) ds, \\ \mathcal{S}_2(x) &= -\Omega^2 D \int_0^x \sin(\sqrt{C}s)(r+s) ds, \\ \mathcal{S}_3(x) &= \beta^3 \int_0^x \sin(\sqrt{C}s)\psi_y\psi_{yy} ds, \\ \mathcal{C}_1(x) &= 2\Omega D \int_0^x \cos(\sqrt{C}s)\psi(s) ds, \\ \mathcal{C}_2(x) &= -\Omega^2 D \int_0^x \cos(\sqrt{C}s)(r+s) ds, \\ \mathcal{C}_3(x) &= \beta^3 \int_0^x \cos(\sqrt{C}s)\psi_y\psi_{yy} ds. \end{aligned}$$

Appendix B. The functions $R_j(x)$

$$\begin{aligned} R_1(x) &= \frac{1}{\sqrt{C}} \{ \sin(\sqrt{C}x) [-\tan(\sqrt{C}l)\mathcal{S}_1(l) - \mathcal{C}_1(l)] \\ &\quad + [\sin(\sqrt{C}x)\mathcal{C}_1(x) - \cos(\sqrt{C}x)\mathcal{S}_1(x)] \}, \\ R_2(x) &= \frac{1}{\sqrt{C}} \{ \sin(\sqrt{C}x) [-\tan(\sqrt{C}l)\mathcal{S}_3(l) - \mathcal{C}_3(l)] \\ &\quad + [\sin(\sqrt{C}x)\mathcal{C}_3(x) - \cos(\sqrt{C}x)\mathcal{S}_3(x)] \}, \\ R_3(x) &= \frac{\beta^2\psi_y^2(l)}{\sqrt{C} \cos(\sqrt{C}l)}, \\ R_4(x) &= \sqrt{C} \{ \sin(\sqrt{C}x) [\tan(\sqrt{C}l)\mathcal{S}_1(l) + \mathcal{C}_1(l)] \\ &\quad + [\cos(\sqrt{C}x)\mathcal{S}_1(x) - \sin(\sqrt{C}x)\mathcal{C}_1(x)] \} \\ &\quad + 2\Omega D\psi(x), \\ R_5(x) &= \sqrt{C} \left\{ \sin(\sqrt{C}x) \left[\tan(\sqrt{C}l)\mathcal{S}_3(l) + \mathcal{C}_3(l) \right. \right. \\ &\quad \left. \left. - \frac{\beta^2\psi_y^2(l)}{2\sqrt{C} \cos(\sqrt{C}l)} \right] \right. \\ &\quad \left. + [\cos(\sqrt{C}x)\mathcal{S}_3(x) - \sin(\sqrt{C}x)\mathcal{C}_3(x)] \right\} \\ &\quad + \beta^3\psi_y\psi_{yy}, \end{aligned}$$

$$R_6(x) = \sqrt{C} \{ \sin(\sqrt{Cx}) [\tan(\sqrt{Cl}) \mathcal{S}_2(l) + \mathcal{C}_2(l)] \\ + [\cos(\sqrt{Cx}) \mathcal{S}_2(x) - \sin(\sqrt{Cx}) \mathcal{C}_2(x)] \} \\ - \Omega^2 D(r+x),$$

$$R_7(x) = \cos(\sqrt{Cx}) [-\tan(\sqrt{Cl}) \mathcal{S}_1(l) - \mathcal{C}_1(l)] \\ + \sin(\sqrt{Cx}) \mathcal{S}_1(x) + \cos(\sqrt{Cx}) \mathcal{C}_1(x),$$

$$R_8(x) = \cos(\sqrt{Cx}) \left[-\tan(\sqrt{Cl}) \mathcal{S}_3(l) - \mathcal{C}_3(l) \right. \\ \left. + \frac{\beta^2 \psi_y^2(l)}{2 \cos(\sqrt{Cl})} \right] \\ + \sin(\sqrt{Cx}) \mathcal{S}_3(x) + \cos(\sqrt{Cx}) \mathcal{C}_3(x),$$

$$R_9(x) = \cos(\sqrt{Cx}) [-\tan(\sqrt{Cl}) \mathcal{S}_2(l) - \mathcal{C}_2(l)] \\ + \sin(\sqrt{Cx}) \mathcal{S}_2(x) + \cos(\sqrt{Cx}) \mathcal{C}_2(x).$$

Appendix C. The functions K_j

$$K_1(x) = \cos(\sqrt{Cx}) [-\tan(\sqrt{Cl}) \mathcal{J}_1(l) - \mathcal{J}_1(l)] \\ + \sin(\sqrt{Cx}) \mathcal{J}_1(x) + \cos(\sqrt{Cx}) \mathcal{J}_1(x),$$

$$K_2(x) = \cos(\sqrt{Cx}) \left[-\tan(\sqrt{Cl}) \mathcal{J}_3(l) - \mathcal{J}_3(l) \right. \\ \left. + \frac{\beta^2 \psi_y^2(l)}{2 \cos(\sqrt{Cl})} \right] \\ + \sin(\sqrt{Cx}) \mathcal{J}_3(x) + \cos(\sqrt{Cx}) \mathcal{J}_3(x),$$

$$K_3(x) = \cos(\sqrt{Cx}) [-\tan(\sqrt{Cl}) \mathcal{J}_4(l) - \mathcal{J}_4(l)] \\ + \sin(\sqrt{Cx}) \mathcal{J}_4(x) + \cos(\sqrt{Cx}) \mathcal{J}_4(x),$$

$$K_4(x, t) = \cos(\sqrt{Cx}) [-\tan(\sqrt{Cl}) \mathcal{J}_2(l) - \mathcal{J}_2(l)] \\ + \sin(\sqrt{Cx}) \mathcal{J}_2(x) + \cos(\sqrt{Cx}) \mathcal{J}_2(x),$$

$$K_5(x) = \sqrt{C} \{ \sin(\sqrt{Cx}) [\tan(\sqrt{Cl}) \mathcal{J}_1(l) + \mathcal{J}_1(l)] \\ + [\cos(\sqrt{Cx}) \mathcal{J}_1(x) - \sin(\sqrt{Cx}) \mathcal{J}_1(x)] \} \\ + 2\Omega D \psi(x),$$

$$K_6(x) = \sqrt{C} \left\{ \sin(\sqrt{Cx}) \left[\tan(\sqrt{Cl}) \mathcal{J}_3(l) + \mathcal{J}_3(l) \right. \right. \\ \left. \left. - \frac{\beta^2 \psi_y^2(l)}{2\sqrt{C} \cos(\sqrt{Cl})} \right] \right. \\ \left. + [\cos(\sqrt{Cx}) \mathcal{J}_3(x) - \sin(\sqrt{Cx}) \mathcal{J}_3(x)] \right\} \\ + \beta^3 \psi_y \psi_{yy},$$

$$K_7(x) = \sqrt{C} \{ \sin(\sqrt{Cx}) [\tan(\sqrt{Cl}) \mathcal{J}_4(l) + \mathcal{J}_4(l)] \\ + [\cos(\sqrt{Cx}) \mathcal{J}_4(x) - \sin(\sqrt{Cx}) \mathcal{J}_4(x)] \} \\ + K\beta^3 \psi_y \psi_{yy},$$

$$K_8(x, t) = \sqrt{C} \{ \sin(\sqrt{Cx}) [\tan(\sqrt{Cl}) \mathcal{J}_2(l) + \mathcal{J}_2(l)] \\ + [\cos(\sqrt{Cx}) \mathcal{J}_2(x) - \sin(\sqrt{Cx}) \mathcal{J}_2(x)] \} \\ + K u_{0,xx},$$

$$K_9(x) = \frac{1}{\sqrt{C}} \{ \sin(\sqrt{Cx}) [-\tan(\sqrt{Cl}) \mathcal{J}_1(l) - \mathcal{J}_1(l)] \\ + [\sin(\sqrt{Cx}) \mathcal{J}_1(x) - \cos(\sqrt{Cx}) \mathcal{J}_1(x)] \},$$

$$K_{10}(x) = \frac{1}{\sqrt{C}} \left\{ \sin(\sqrt{Cx}) \left[-\tan(\sqrt{Cl}) \mathcal{J}_3(l) \right. \right. \\ \left. \left. - \mathcal{J}_3(l) + \frac{\beta^2 \psi_y^2}{2 \cos(\sqrt{Cl})} \right] \right. \\ \left. + [-\cos(\sqrt{Cx}) \mathcal{J}_3(x) + \sin(\sqrt{Cx}) \mathcal{J}_3(x)] \right\},$$

$$K_{11}(x) = \frac{1}{\sqrt{C}} \{ \sin(\sqrt{Cx}) [-\tan(\sqrt{Cl}) \mathcal{J}_4(l) - \mathcal{J}_4(l)] \\ + [-\cos(\sqrt{Cx}) \mathcal{J}_4(x) + \sin(\sqrt{Cx}) \mathcal{J}_4(x)] \},$$

$$K_{12}(x, t) = \frac{1}{\sqrt{C}} \{ \sin(\sqrt{Cx}) [-\tan(\sqrt{Cl}) \mathcal{J}_5(l) - \mathcal{J}_5(l)] \\ + [\sin(\sqrt{Cx}) \mathcal{J}_5(x) - \cos(\sqrt{Cx}) \mathcal{J}_5(x)] \},$$

where we have

$$\mathcal{J}_1(x) = 2\Omega D \int_0^x \sin(\sqrt{Cs}) \psi(s) ds,$$

$$\mathcal{J}_2(x, t) = K \int_0^x \sin(\sqrt{Cs}) u_{0,xx} ds,$$

$$\mathcal{I}_3(x) = \beta^3 \int_0^x \sin(\sqrt{C}s) \psi_{,y} \psi_{,yy} ds,$$

$$\mathcal{I}_4(x) = K\beta^3 \int_0^x \sin(\sqrt{C}s) \psi_{,y} \psi_{,yy} ds,$$

$$\mathcal{I}_5(x, t) = K \int_0^x \sin(\sqrt{C}s) u_{0,xtt} ds,$$

$$\mathcal{I}_1(x) = 2\Omega D \int_0^x \cos(\sqrt{C}s) \psi(s) ds,$$

$$\mathcal{I}_2(x, t) = K \int_0^x \cos(\sqrt{C}s) u_{0,xtt} ds,$$

$$\mathcal{I}_3(x) = \beta^3 \int_0^x \cos(\sqrt{C}s) \psi_{,y} \psi_{,yy} ds,$$

$$\mathcal{I}_4(x) = K\beta^3 \int_0^x \cos(\sqrt{C}s) \psi_{,y} \psi_{,yy} ds,$$

$$\mathcal{I}_5(x, t) = K \int_0^x \cos(\sqrt{C}s) u_{0,xtt} ds.$$

References

- [1] G.D. Padfield, Helicopter Flight Dynamics, Blackwell Science, Cambridge, 1996.
- [2] P.P. Friedmann, T.A. Millott, Vibration reduction in rotorcraft using active control: a comparison of various approaches, J. Guidance, Control Dyn. 18 (1995) 664.
- [3] L. Meirovitch, Hybrid state equations of motion for flexible bodies in terms of quasicordinates, J. Guidance, Control Dyn. 14 (1991) 1008.
- [4] L. Meirovitch, T. Stemple, Hybrid equations of motion for flexible multibody systems using quasicordinates, J. Guidance, Control Dyn. 18 (1995) 678.
- [5] M.A. Jalali, B. Mehri, Periodicity and chaos in a flexible crank-rocker mechanism, Int. J. Non-Linear Mech. 34 (1999) 1103.
- [6] E. Esmailzadeh, M.A. Jalali, Nonlinear oscillations of viscoelastic rectangular plates, Nonlinear Dyn. 18 (1999) 311.
- [7] J.G. Leishman, Principles of Helicopter Aerodynamics, Cambridge University Press, Cambridge, 2000.
- [8] C.Y. Chia, Nonlinear Analysis of Plates, McGraw-Hill, New York, 1980.
- [9] Y.C. Fung, Foundations of Solid Mechanics, Prentice-Hall, Englewood Cliffs, NJ, 1965.
- [10] J. Argyris, G. Faust, M. Haase, An Exploration of Chaos, Elsevier, Amsterdam, 1994.
- [11] J.N. Reddy, Applied Functional Analysis and Variational Methods in Engineering, McGraw-Hill, New York, 1986.
- [12] F. Verhulst, Nonlinear Differential Equations and Dynamical Systems, Springer, Berlin, 1990.
- [13] C.L. Siegel, J. Moser, Lectures on Celestial Mechanics, Springer, Berlin, 1971.
- [14] P.J. Holmes, A nonlinear oscillator with a strange attractor, Philos. Trans. R. Soc. London 292 (1394) (1979) 419.
- [15] E.K. Hall II, S.V. Hanagud, Control of nonlinear structural dynamic systems: chaotic oscillations, J. Guidance, Control Dyn. 16 (1993) 470.